Annex

Climate change impacts on glaciers and water resources in the headwaters of the Tarim River, NW China/Kyrgyzstan

Michel Wortmann[1,*], Doris Duethmann[2,3], Christoph Menz[1], Tobias Bolch[4,5], Shaochun Huang[1,6], Jiang Tong[7], Zbigniew W. Kundzewicz[1,8] and Valentina Krysanova[1]

1 Methods

1.1. SWIM-G glacier processes

Mass balance accounting is achieved by SWIM's enhanced Degree-Day snowmelt module (Huang et al., 2013) and Degree-Day ice melting, with melt rates changing with aspect (includes terrain shading) and debris cover. The snowpack is transferred to the glacier dynamics module if the critical height (dependent on slope) is exceeded at the end of the melting season. The ice is then subject to lateral, downstream flow according to an approach based on Glen's Flow Law (Marshall et al., 2011; Cuffey and Paterson, 2010). Avalanching occurs if the slope exceeds a critical limit. Two other processes often neglected in large-scale glacio-hydrological models are considered in SWIM-G because they play a major role in the Tarim headwaters: sublimation and debris cover. Although it is often a negligible mass balance component, sublimation becomes important in dry and high elevation zones such as the Tibetan Plateau or the Karakoram (Zhang et al., 2006; Mölg et al., 2009). Debris thickness on glaciers has been shown to exponentially decrease ablation rates (Mattson, 1993; Nicholson and Benn, 2006). Thickness generally increases with negative mass balances as englacial debris is left behind, providing a shield and a negative feedback under a warmer climate. To capture this effect, a debris concentration approach is implemented that alters the height according to the specific mass balance including 'dilution' by ice flow (similar to Bozhinskiy et al., 1986). Hagg et al. (2008) studied subdebris melt rates for the largest glacier of the Tien Shan, the heavily debris-covered South Inylchek glacier, Kyrgyzstan, in the Aksu catchment. Their findings are used here to alter the melt factors via the accepted negative exponential relationship with height.

1.2. SWIM-G calibration/validation results

Calibration are given in Table A1 and Figure A1. By applying the thresholds shown in the table header, the 100 Pareto-optimal calibrations are reduced to number N. The NSE_c is given for the calibration and the validation years. Following the split- sample calibration–validation approach, the available discharge data were split into 4-yr periods (the calendar years 1964–87, yielding six periods). The model was calibrated to all odd-numbered periods (1964–67, 1972–75, 1980–83) and validated to the even-numbered periods (1968–71, 1976–79, 1984–87). In the Hotan and Yarkant catchments, median values are provided for the most plausible mass balance scenario with a residual mass balance parameter value of b_r=-0.1m weq. a^{-1}, as it best matches mass balance assessments in these catchments from the 2000s. This method was preferred, because the day-to-day correlation of the precipitation data with discharge was found to be worse in the 1980s than in the 1970s (most likely caused by changes in meteorological station density). This meant that choosing either decade as the calibration or vali- dation period would distort the results of the validation.

Table A1: Model performance according to the median values of the four objective functions over the calibration ensemble (N: number of calibration members meeting the minimum threshold, NSE_c: the combined normal and logged Nash-Sutcliffe Efficiency, $RMSE_{QA}$: root mean square error of mean annual discharge, X^2: match between simulated and observed glacier hypsometry, MB_Y: mass balance error probability).

	N	NSE_c		$RMSE_{QA}$	X^2	MB_Y
		cal.	val.	%	%	
threshold		0.6		25	20	0.05
Aksu						
Xiehela	100	0.936	0.889	13.4	8.4	0.001
Shaliguilanke	49	0.827	0.787	16.3	14.7	0.023
Hotan						
Wuluwati	67	0.734	0.696	20.1	11.8	
Tongguziluoke	83	0.765	0.728	21.1	4	
Yarkant						
Kaqun	97	0.856	0.813	16.6	11.1	

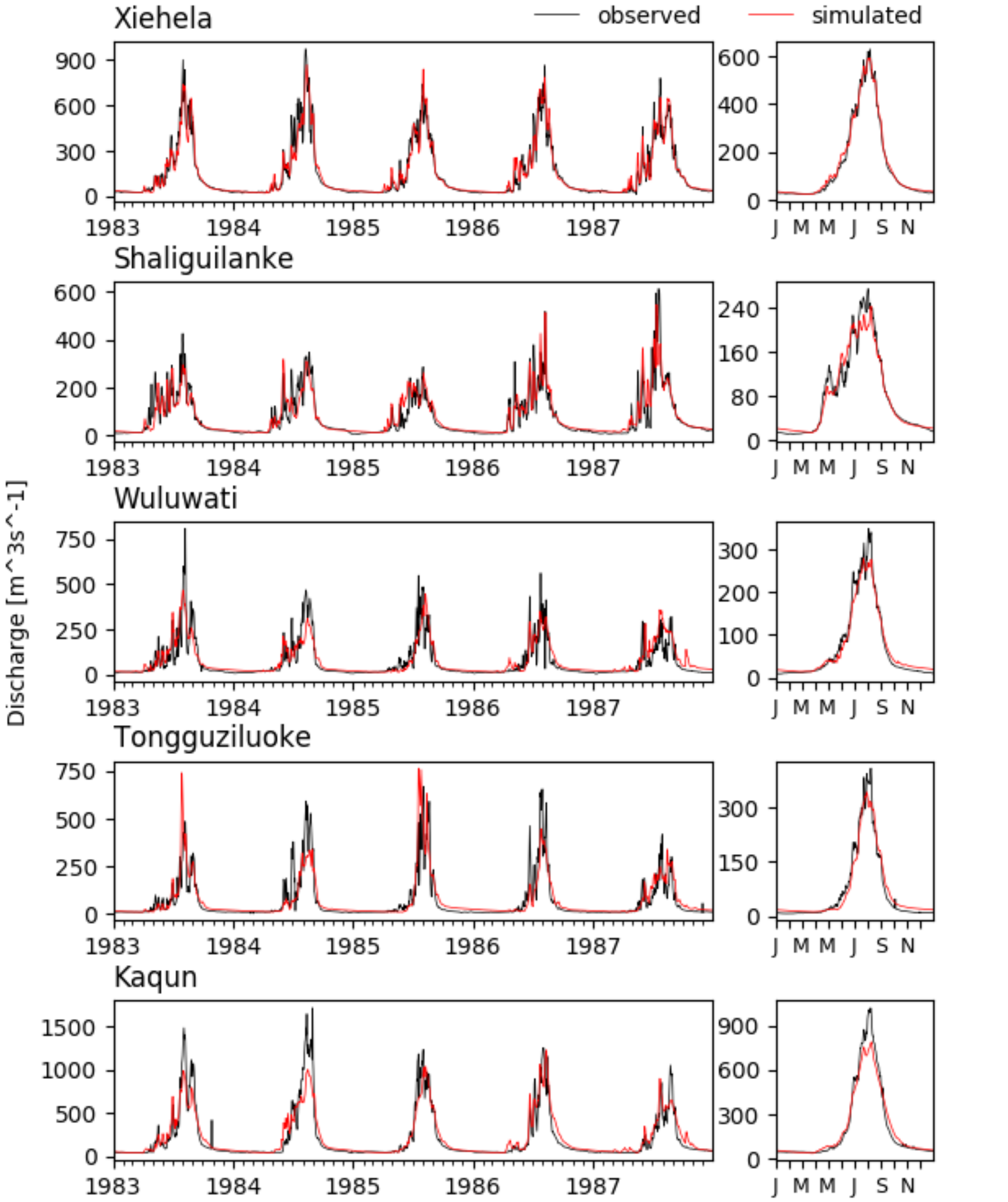

Figure A1: SWIM-G simulated (red) and observed (black) daily discharge in the calibration and validation periods (see Section 1.2 for details on periods). The day-of-year mean is for all years with available observations (~1964-1987), while the daily plots for the years 1983-1987 was chosen to show the daily dynamics.

1.3. SWIM-G parameter set selection

Figure A2: Exemplary plot of model solutions to illustrate the selection of parameter sets for the impact assessment. All dots are positioned on an idealised Pareto front. The best performing sets for each objective function was chosen as well as the best tradeoff. Choosing the best performing parameter sets ensures that the full range of model performances is covered because the best set according to one objective function is simultaneously the worst of another. The best tradeoff parameter set has the minimum distance to the origin (d) after the axes have been scaled to the highest (i.e. worst) value of its objective function. The model used in this study used four (three) objective functions in the Aksu (Hotan and Yarkant) catchments. Thus, the selection yields five (four) parameter sets. As no long-term, catchment-wide mass balance measurements are available for the Hotan and Yarkant catchments, the most plausible scenario (residual mass balance b_r=-0.1m, see Wortmann et al., 2018) was chosen, i.e. the one fitting best to recent observations from the 2000s.

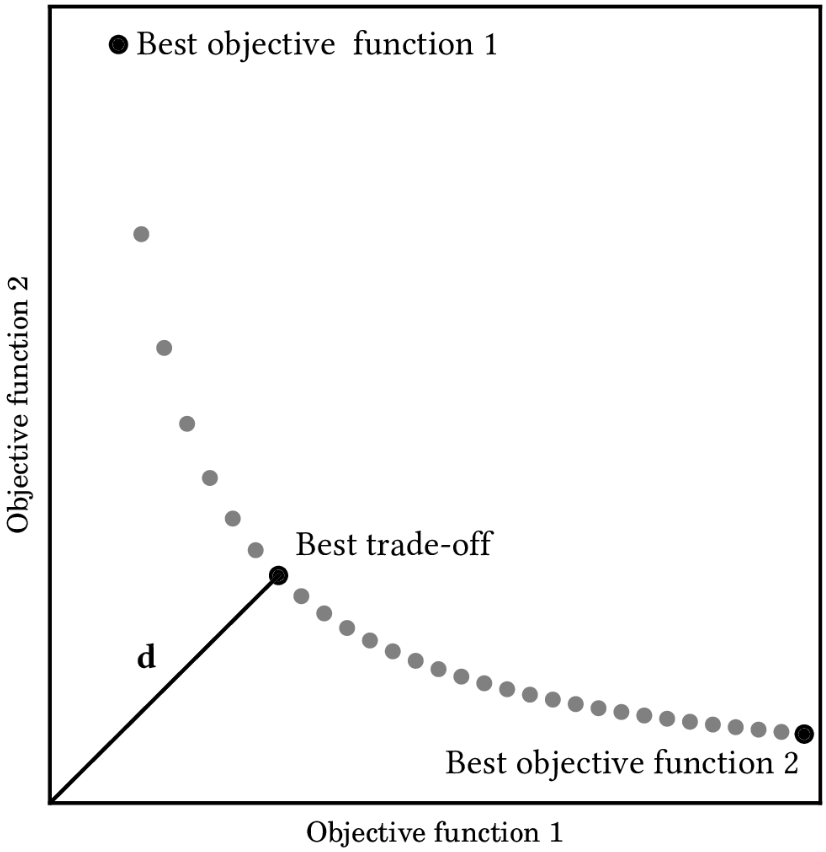

1.4. WASA glacio-hydrological processes

Precipitation is differentiated as snow or rain depending on whether the air temperature exceeds a calibrated threshold temperature. The spatial variability of snow within an elevation zone is represented by a snow depletion curve (Liston, 2004). Snow is further redistributed from higher to lower elevation zones if simulated snow outside a glacier accumulates above a given snow water equivalent threshold. Snow and glacier melt are calculated using the temperature-index approach

(Hock, 2003). The seasonal variation in incoming solar radiation is considered by a melt factor that varies in a sinusoidal form between a minimum value at the winter solstice and a maximum value at the summer solstice (Anderson, 1973). Glacier area and surface elevation changes are simulated using the Δh-approach by Huss et al. (2010) and updated annually. Glaciers are considered individually and discretized into elevation bands. Thickness changes in each elevation band are calculated using predefined functions derived from observed glacier thickness changes. The glacier area is reduced if the thickness change in an elevation band is higher than the remaining ice thickness. Interception and evapotranspiration are calculated with the Penman-Monteith equation (Monteith, 1965) and the two-layer model of Shuttleworth and Wallace (1985). The model simulates infiltration with the Green-Ampt approach (Green and Ampt, 1911). Runoff is generated from surface runoff, interflow and groundwater.

1.5. WASA calibration results

The simulated glacier mass balance (with respect to the glacier area) in the Aksu basin over the period 1961-2001 was −0.41 m w.e.q. a^{-1} (Xiehela) and −0.42 m w.e.q. a^{-1} (Shaliguilanke). For the Aksu catchment, the glacier area change during the observed period was given and not simulated. The simulated glacier mass balance in the Hotan and Yarkand basins was much less negative with −0.10, −0.11, and −0.10 m w.e.q. a^{-1} for Wuluwati, Tonguziluoke, and Kaqun, respectively. Glacier area changes during this period were −2% (Wuluwati), −7.9% (Tonguziluoke), and −4.2% (Kaqun).

Table A2: Performance of the hydrological model WASA during the calibration and validation periods. Shown are the Nash-Sutcliffe efficiency (Eff), the Nash-Sutcliffe efficiency for log discharge values (Log Eff), and the volume bias (Bias) for daily and monthly time series.

			Calibration period			Evaluation period		
Basin	Gauge		Eff	Log Eff	Bias	Eff	Log Eff	Bias
Aksu	Xiehela	daily	0.85	0.95	0.05	0.84	0.94	0.07
		monthly	0.93	0.97	0.08	0.93	0.97	0.08
	Shaliguilanke	daily	0.80	0.85	-0.04	0.79	0.85	-0.03
		monthly	0.87	0.89	-0.03	0.87	0.89	-0.03
Hotan	Tonguziluoke	daily	0.60	0.82	-0.14	0.72	0.87	-0.11
		monthly	0.74	0.87	-0.14	0.83	0.91	-0.11
	Wuluwati	daily	0.67	0.71	-0.13	0.71	0.68	-0.13
		monthly	0.83	0.78	-0.14	0.83	0.75	-0.13
Yarkant	Kaqun	daily	0.75	0.83	-0.13	0.74	0.83	-0.12
		monthly	0.81	0.87	-0.13	0.81	0.87	-0.12

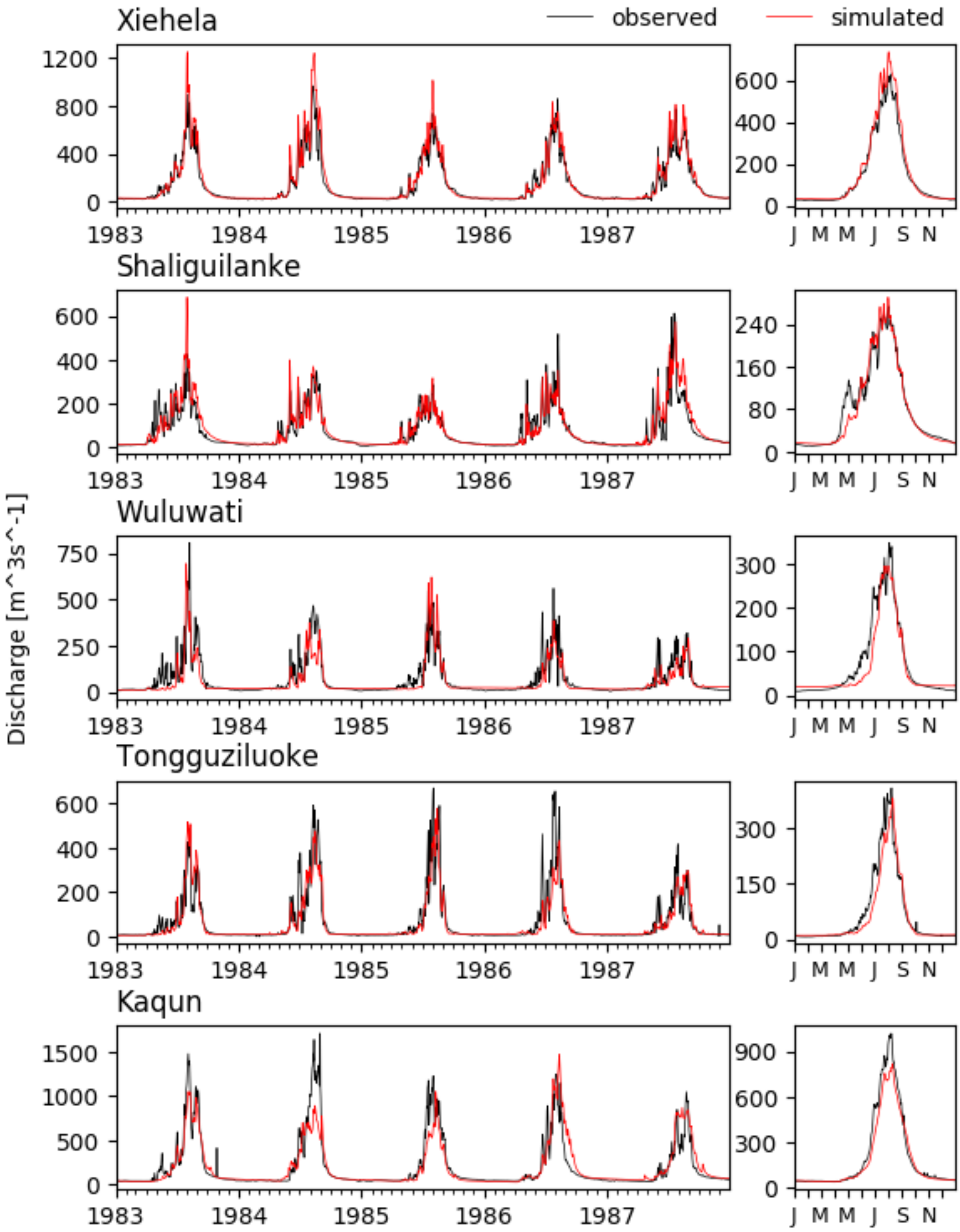

Figure A3: WASA simulated (red) and observed (black) daily discharge. The day-of-year mean is for all years with available observations (~1964-1987), while the daily plots for the years 1983–1987 (which are within the calibration period) was chosen to show the daily dynamics (left panel).

1.6. Selected GCM results

Table A3: List of selected GCMs whose output is used for the climate impact assessment. Ensemble position refers to the tendency compared to the other models with regards to temperature and precipitation.

Model name	Institute
CNRM-CM5	Centre National de Recherches Meteorologiques, France
GFDL-ESM2M	Geophysical Fluid Dynamics Laboratory, US
HadGEM2-ES	Met Office Hadley Centre, UK
IPSL-CM5A-LR	Institut Pierre-Simon Laplace, France
MIROC5 MIROC-ESM-CHEM MIROC-ESM	Japan Agency for Marine-Earth Science and Technology, Atmosphere and Ocean Research Institute
MRI-CGCM3	Meteorological Research Institute, Japan

2 Additional results

Table A4 Ensemble median values and standard deviations (after ±) of the glacier area change (%) projections compared to the reference period (1971-2000) over the three future climate periods for SWIM-G (1) and WASA (2).

Catchment		2011-2040			2041-2070			2071-2100		
RCP		2.6	4.5	8.5	2.6	4.5	8.5	2.6	4.5	8.5
Xiehela	1)	-11±05	-10±05	-11±06	-25±09	-23±11	-29±11	-32±12	-37±13	-50±13
	2)	-7±02	-6±02	-7±03	-23±12	-21±16	-33±18	-39±16	-47±21	-71±18
Shalig.	1)	-21±09	-21±08	-21±09	-42±14	-41±15	-48±14	-51±18	-57±17	-75±13
	2)	-11±06	-10±05	-10±06	-42±17	-40±19	-51±18	-60±18	-64±19	-84±12
Wuluwati	1)	-8±07	-6±06	-9±05	-23±15	-25±14	-31±15	-35±19	-48±19	-61±19
	2)	0±00	0±00	0±00	-7±03	-7±02	-9±03	-16±06	-21±07	-29±11
Tongguz.	1)	-3±04	-2±04	-3±04	-10±11	-11±11	-14±12	-16±16	-24±17	-34±21
	2)	0±00	0±00	0±00	-3±02	-3±02	-3±02	-8±05	-10±5	-14±07
Kaqun	1)	-7±04	-8±05	-9±04	-22±10	-23±10	-28±10	-35±13	-46±15	-58±17
	2)	0±00	0±00	-1±00	-10±04	-10±04	-12±05	-25±08	-32±11	-45±16

1) SWIM-G, 2) WASA

Table A5: Ensemble median values and standard deviations (after ±) of glacier volume change (%) projections compared to the reference period (1971-2000) over the three future climate periods for SWIM-G (1) and WASA (2).

Catchment		2011-2040			2041-2070			2071-2100		
	RCP	2.6	4.5	8.5	2.6	4.5	8.5	2.6	4.5	8.5
Xiehela	1)	-15±07	-14±07	-15±08	-29±11	-28±13	-34±12	-34±14	-41±15	-56±14
	2)	-23±07	-22±06	-23±07	-53±13	-51±13	-59±12	-63±12	-68±11	-79±09
Shalig.	1)	-25±12	-24±11	-24±11	-51±17	-49±16	-58±15	-61±20	-67±17	-81±10
	2)	-32±11	-31±10	-31±10	-70±16	-67±15	-75±14	-83±15	-86±13	-97±09
Wuluwati	1)	-13±9	-10±09	-14±07	-29±17	-32±16	-38±17	-41±20	-54±20	-66±19
	2)	-12±04	-11±03	-12±03	-25±08	-27±08	-30±08	-37±12	-44±13	-52±14
Tongguz.	1)	-4±06	-3±06	-5±06	-12±15	-14±14	-18±16	-18±20	-28±20	-39±23
	2)	-6±02	-5±02	-6±02	-12±05	-13±04	-14±05	-18±07	-21±07	-26±09
Kaqun	1)	-9±07	-10±07	-12±06	-28±14	-30±13	-35±13	-40±16	-53±17	-65±18
	2)	-12±04	-12±04	-13±03	-30±09	-31±09	-35±10	-45±13	-52±14	-62±15

1) SWIM-G, 2) WASA

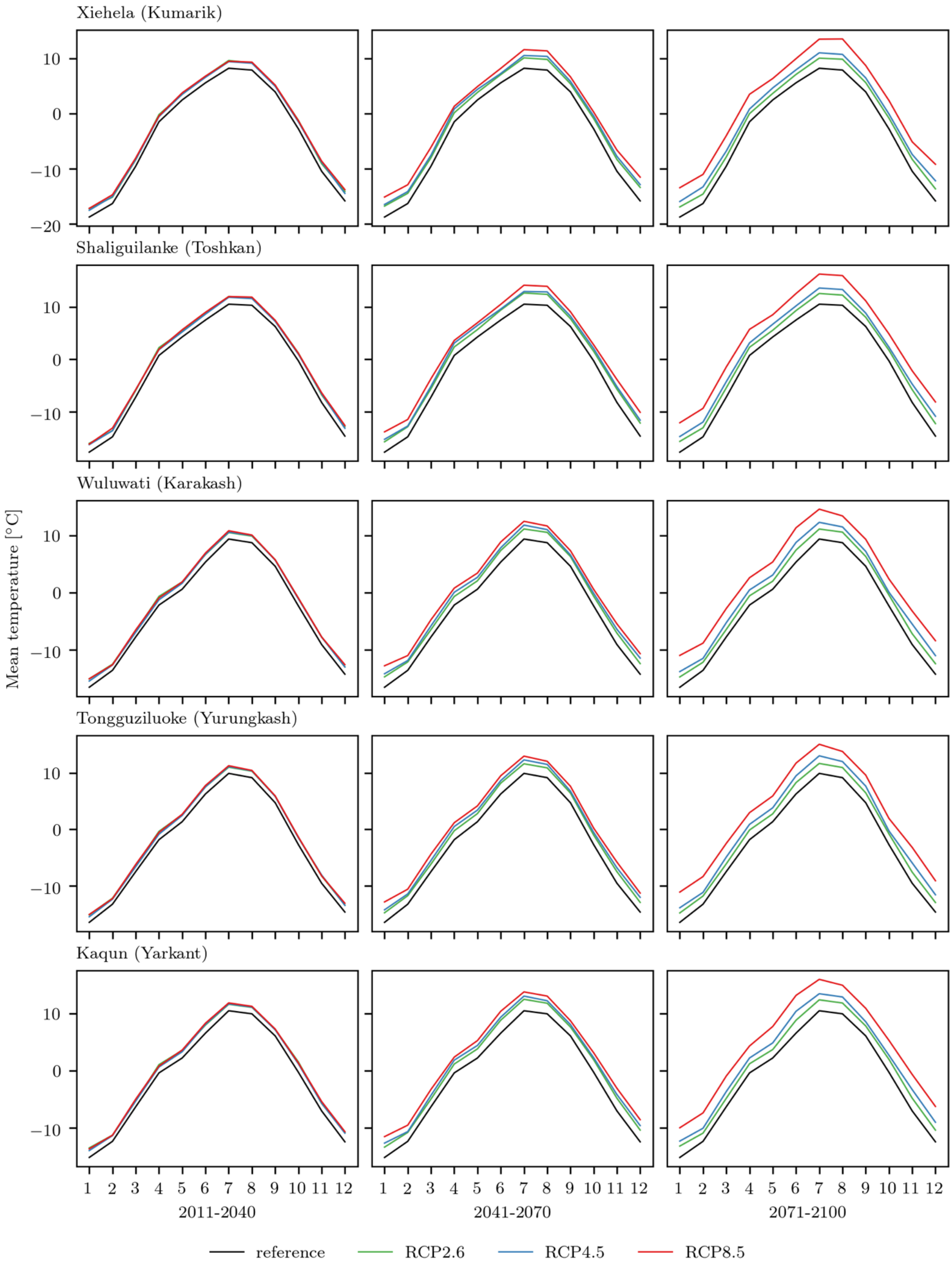

Figure A4: Mean monthly temperature (ensemble median) in all five catchments for the three scenarios and three future periods compared to the reference period (black line). Annual and period means as well as the ensemble spread is shown in Figure 2 in the manuscript.

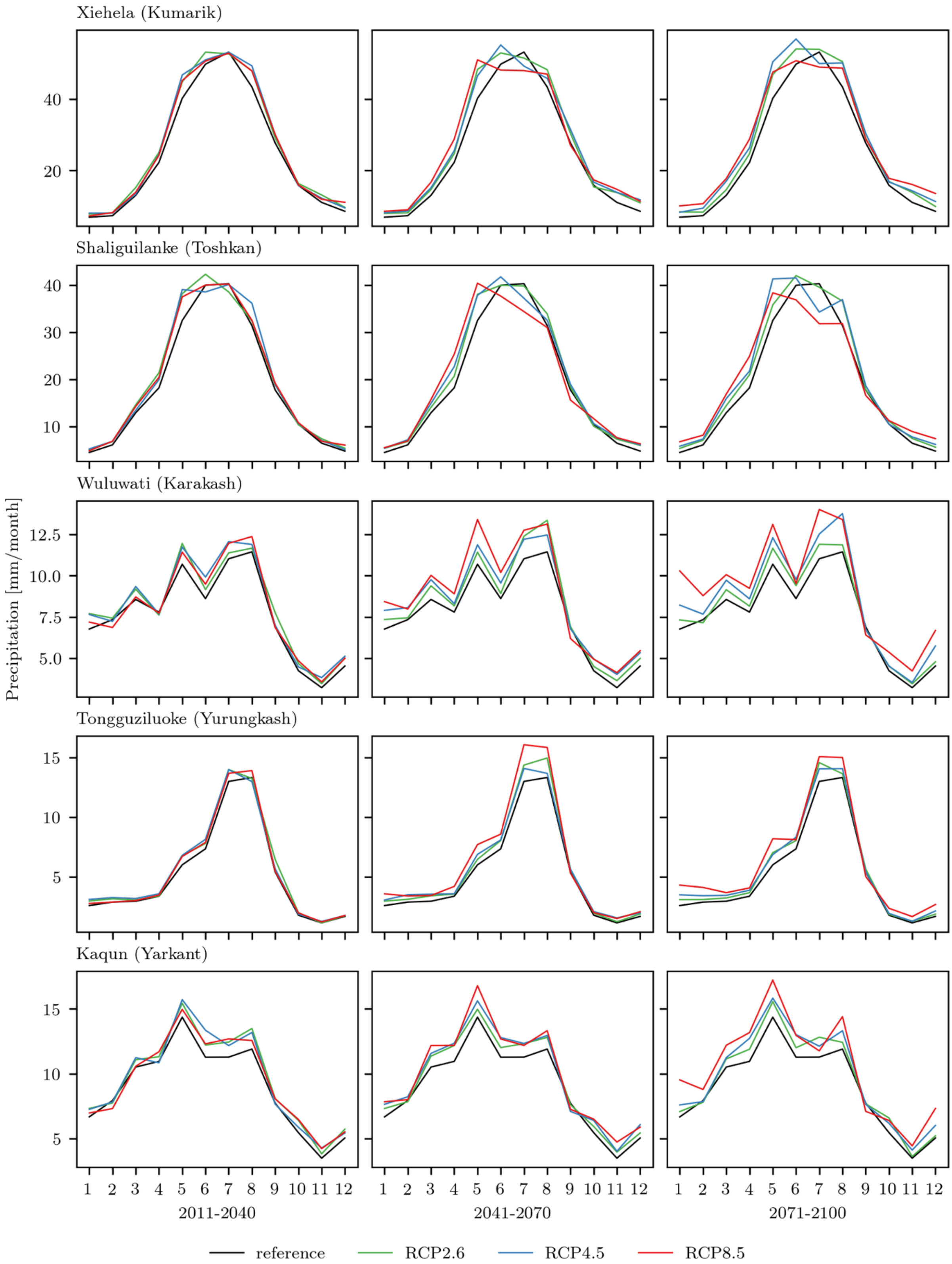

Figure A5: Mean monthly precipitation (uncorrected, ensemble median) in all five catchments for the three scenarios and three future periods compared to the reference period (black line). Annual and period means as well as the ensemble spread is shown in Figure 2 in the manuscript.

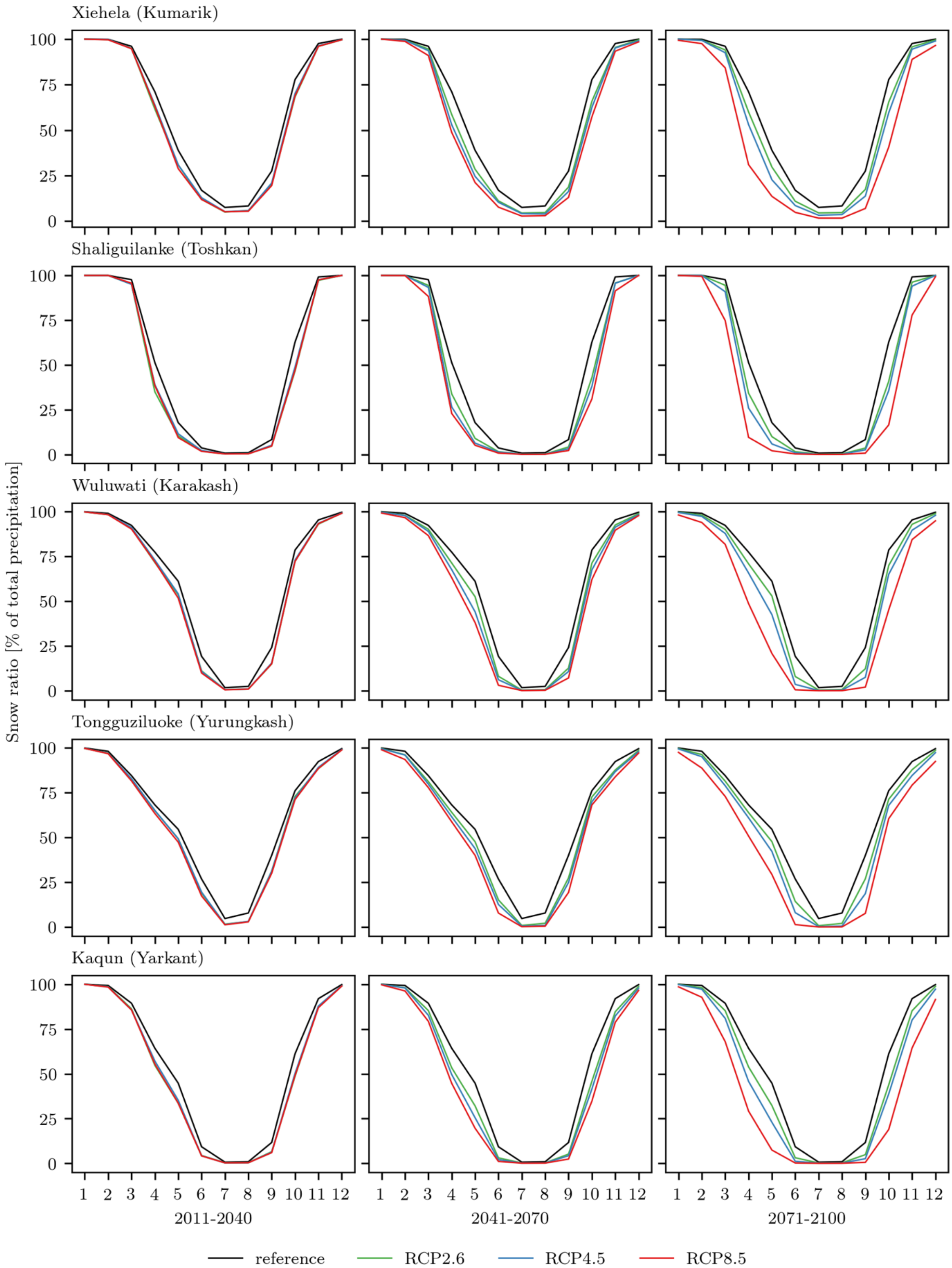

Figure A6: Mean monthly snow fraction (snow/precipitation, ensemble median) in all five catchments for the three scenarios and three future periods compared to the reference period (black line).

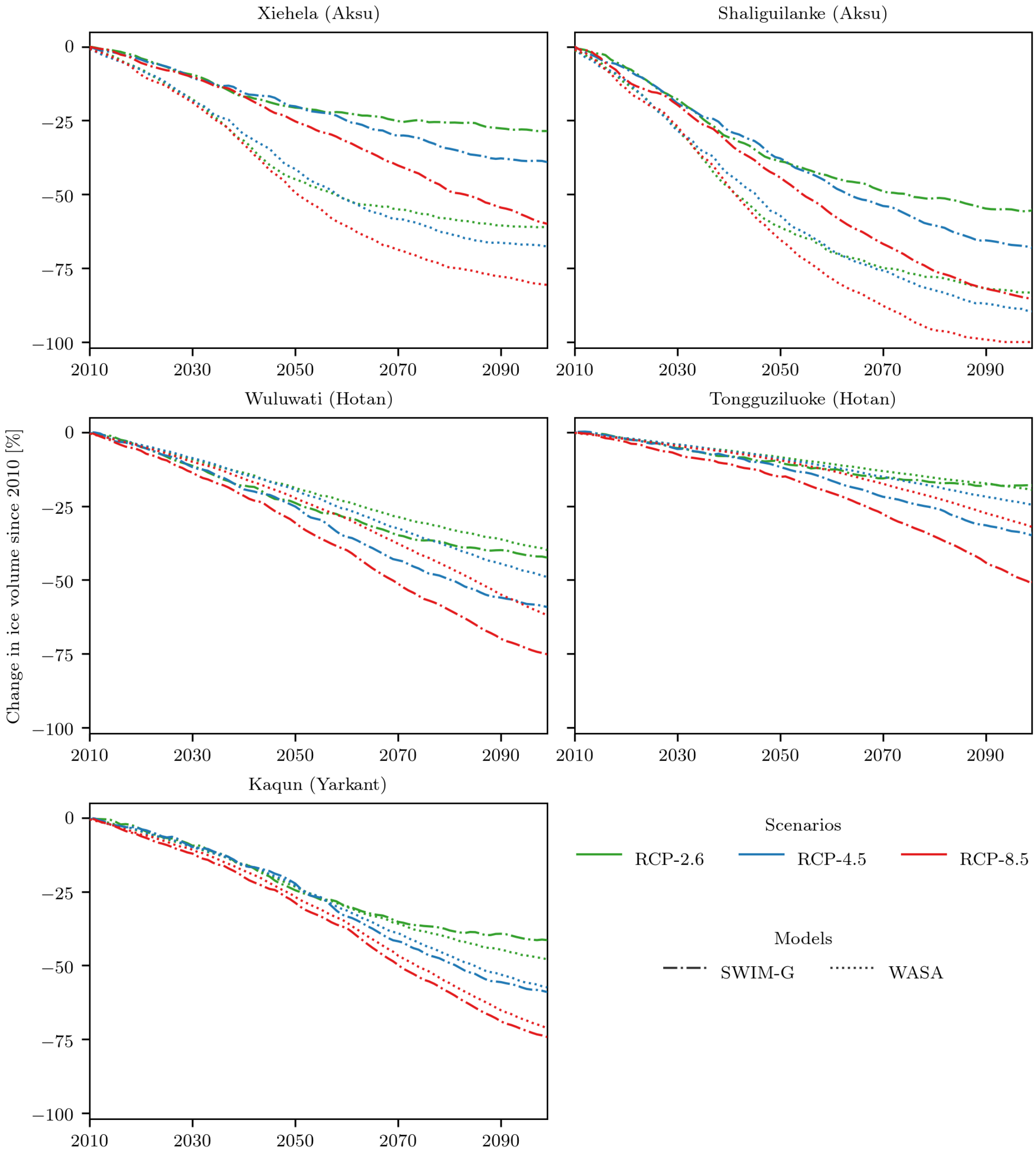

Figure A6: Same as in Figure 3 in the article but for glacier volume (water equivalents) changes.

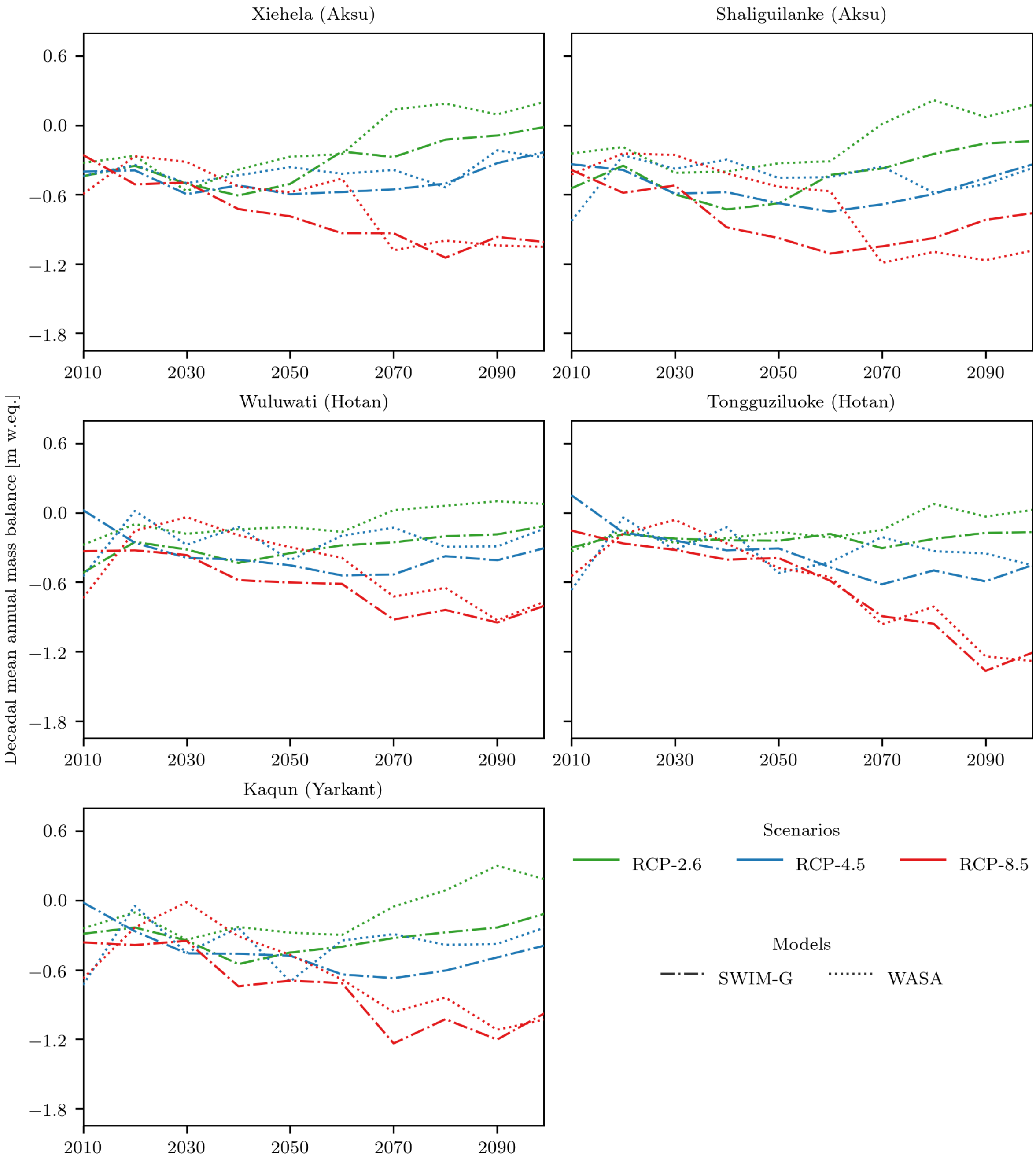

Figure A7: Same as in Figure 3 in the article but for decadal mean mass balances.

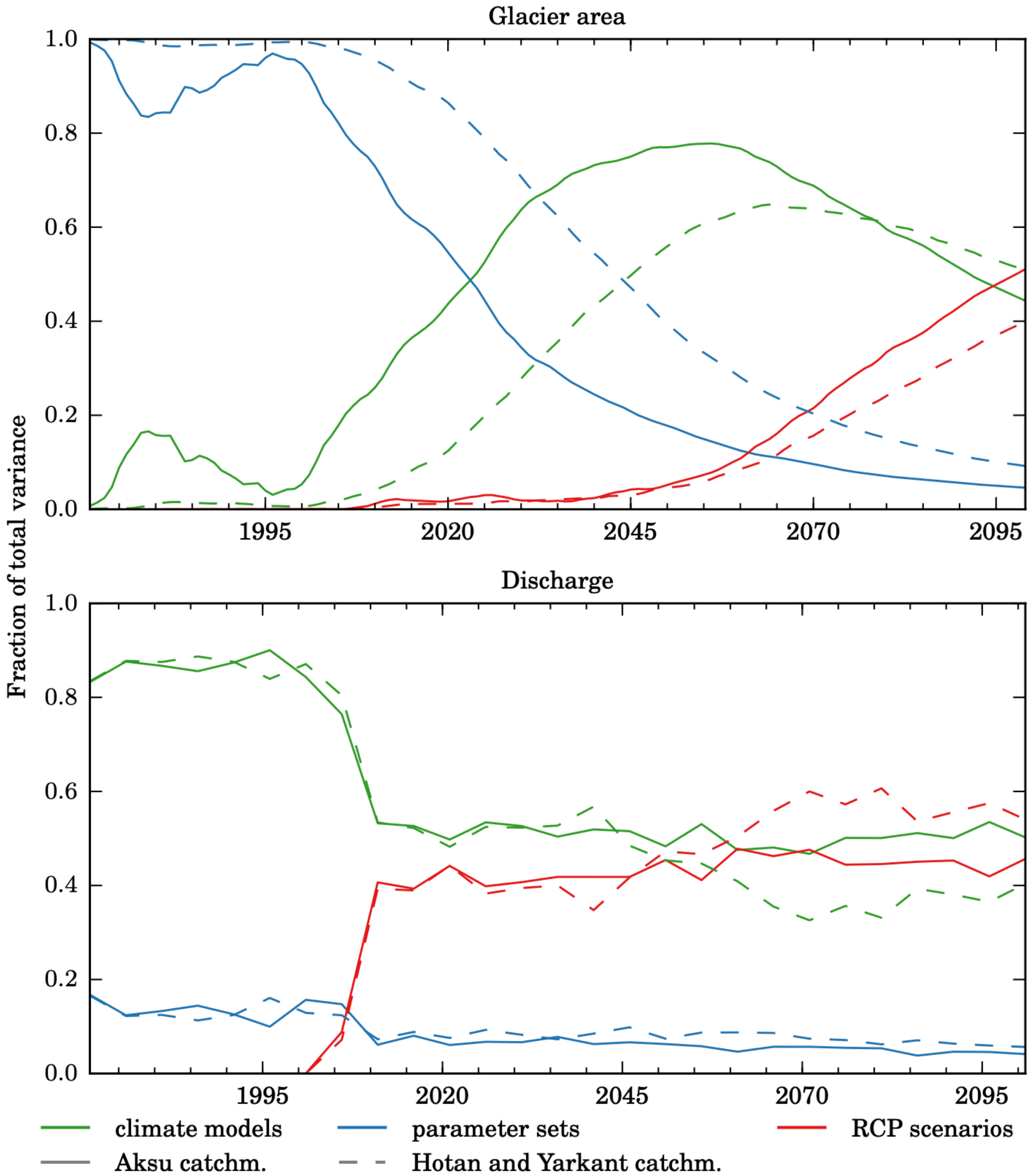

Figure A8: Analysis of variance (ANOVA, Gottschalk, 2006) of glacier area and discharge simulations by SWIM-G. The model was driven by the climate model ensemble with several scenarios as well as with different glaciohydrological model parameter sets (as described in Section A2). The plots reveal the different sources of uncertainty over the reference period (until 2000) and projections.

Additional references in Annex

Anderson, E. A. 1973. National Weather Service river forecast system - Snow accumulation and ablation model, U.S. Dep. of Commer. NOAA NWS, Washington, D.C., Technical Memorandum NWS HYDRO-17, 217.

Bosshard, T., M. Carambia, K. Goergen et al., 2013. Quantifying uncertainty sources in an ensemble of hydrological climate-impact projections. Water Resources Research, 49(3):1523–1536.

Bozhinskiy, A., M. Krass, V. Popovnin 1986. Role of debris cover in the thermal physics of glaciers. Journal of Glaciology, 32:255–266.

Chaturvedi, R. K., A. Kulkarni, Y. Karyakarte et al., 2014. Glacial mass balance changes in the Karakoram and Himalaya based on CMIP5 multi-model climate projections. Climatic Change, 123(2):315–328.

Cuffey, K. M., W. S. B. Paterson 2010. The Physics of Glaciers. Amsterdam: Elsevier. 00292.

Fan, Y., Y. Chen, W. Li, H. Wang, X. Li 2011. Impacts of temperature and precipitation on runoff in the Tarim River during the past 50 years. Journal of Arid Land, 3:220–230.

Gan, R., Y. Luo, Q. Zuo, L. Sun 2015. Effects of projected climate change on the glacier and runoff generation in the Naryn River Basin, Central Asia. Journal of Hydrology, 523:240–251.

Gelfan, A., J. Pomeroy, L. Kuchment 2004. Modeling forest cover influences on snow accumulation, sublimation, and melt. Journal of Hydrometeorology, 5(5):785–803.

Green, W., and Ampt, G. 1911. Studies on soil physics Part I - The flow of air and water through soils, J. Agr. Sci., 4, 1-24.

Hagg, W., M. Hoelzle, S. Wagner et al., 2013. Glacier and runoff changes in the Rukhk catchment, upper Amu-Darya basin until 2050. Global and Planetary Change, 110:62–73.

Hagg, W., C. Mayer, A. Lambrecht, A. Helm 2008. Sub-Debris Melt Rates on Southern Inylchek Glacier, Central Tian Shan. Geografiska Annaler: Series A, Physical Geography, 90(1):55–63.

Hattermann, F., M. Weiland, S. Huang et al., 2011. Model-Supported Impact Assessment for the Water Sector in Central Germany Under Climate Change—A Case Study. Water Resources Management, 25(13):3113–3134.

Hattermann, F. F., M. Wattenbach, V. Krysanova, F. Wechsung 2005. Runoff simulations on the macroscale with the ecohydrological model SWIM in the Elbe catchment-validation and uncertainty analysis. Hydrological Processes, 19(3):693–714.

Hock, R. (2003). Temperature index melt modelling in mountain areas, J. Hydrol., 282, 104-115, 10.1016/s0022-1694(03)00257-9.

Koch, H., S. Liersch, and F. F. Hattermann 2013. Integrating water resources management in eco-hydrological modelling. Water Science & Technology, 67(7).

Kulkarni, A. 2014. Glaciers as source of water: The Himalaya. In Sustainable Humanity, Sustainable Nature: Our Responsibility, number 41 in Pontifical Academy of Sciences Extra Series. Vatican City: Pontifical Academy of Sciences.

Liersch, S., J. Cools, B. Kone et al., 2012. Vulnerability of rice production in the Inner Niger Delta to water resources management under climate variability and change. Environmental Science & Policy.

Liston, G. E. (2004). Representing subgrid snow cover heterogeneities in regional and global models, J. Clim., 17, 1381-1397, 10.1175/1520-0442(2004)017<1381:rsschi>2.0.co;2.

Lutz, A. F., W. W. Immerzeel, A. Gobiet et al., 2013. Comparison of climate change signals in CMIP3 and CMIP5 multi-model ensembles and implications for Central Asian glaciers. Hydrol. Earth Syst. Sci., 17(9):3661–3677.

Marshall, S. J., E. C. White, M. N. Demuth et al., 2011. Glacier Water Resources on the Eastern Slopes of the Canadian Rocky Mountains. Canadian Water Resources Journal / Revue canadienne des ressources hydriques, 36(2):109–134.

Mattson, L. 1993. Ablation on debris covered glaciers: An example from the Rakhiot Glacier, Panjab, Himalaya. IAHS publication, 218:289–296. 00125.

Mölg, T., N. J. Cullen, and G. Kaser 2009. Solar radiation, cloudiness and longwave radiation over low-latitude glaciers: Implications for mass-balance modelling. Journal of Glaciology, 55(190):292–302.

Monteith, J. L. 1965. Evaporation and environment, Symo. Soc. Exp. Biology, 19, 205-234.

Moss, R. H., J. A. Edmonds, K. A. Hibbard et al, 2010. The next generation of scenarios for climate change research and assessment. Nature, 463(7282):747–756.

Nicholson, L. and D. I. Benn 2006. Calculating ice melt beneath a debris layer using meteorological data. Journal of Glaciology, 52(178):463–470. 00078.

Shuttleworth, W. J., and Wallace, J. S. 1985. Evaporation from sparse crops - an energy combination theory, Q. J. Roy. Meteor. Soc., 111, 839-855, 10.1256/smsqj.46909.